S&G 3681

Comparison of Linear and Non-Linear Seismic Response of 2-Dimensional Alluvial Basins

by

A.J. Haines[#], R.A. Benites[#], J. Marsh[+] and T.J. Larkin[+]

Institute of Geological and Nuclear Sciences Limited, P.O. Box 1320, Wellington, New Zealand.

+ Department of Civil Engineering, University of Auckland, Private Bag 92019, Auckland, New Zealand.

1. INTRODUCTION

Both geological and topographical conditions are known to strongly influence the nature of ground motion at a site. In particular, soft sediment filled basins may cause significant amplification of earthquake motions due to wave phenomena such as focusing and resonance.

Recent large magnitude events, like the 1985 Michoacan (Mexico) earthquake and the 1989 Loma Prieta (California, U.S.A.) earthquake, have highlighted the amplification effects produced by deposits of alluvium of relatively shallow depths, e.g. 20 - 30 metres. The Loma Prieta earthquake in particular showed the existence of significant "site effects" with surface accelerations at sites interlaid by alluvium being two or three times that recorded at closely adjacent rock sites. It also showed strong evidence that the amplification factors in soft sediments are much larger for weak motion than for strong motion, both recorded at the same site (Darragh and Shakal 1991). Such an effect is not observed for stiffer soils. From similar observations at sites on Franciscan rock and nearby sediments it is evident that differences in amplification factors between strong and weak motions start to appear at acceleration levels greater than $0.1g$ to $0.3g$, and it is suggested that this effect is due to nonlinear response of the sediment sites (Chin and Aki 1991).

In the past two decades considerable effort has been devoted to develope modelling techniques of seismic wave propagation in complex media to study the effect of the geological site conditions on the ground motion. Most of the techniques assume a linear relationship of stress and strain, while others consider either that the stress-strain relationship of soils may depend on the intensity of the confining pressure or that shearing nonlinear behaviour will appear as result of large shear inputs. Linear models have been developed extensively for two-dimensional structures, and the general features of the 2-D seismic response are well established (Aki, 1988). To much lesser extent the linear models for three-dimensional structures are developed at present, and the reader is refered to the pioneer work of Lee (1978, 1984), Lee and Langston (1983), Sanchez-Sesma (1983), and Mossessian and Dravinski (1989, 1990). The case of nonlinearity has been studied mainly by geotechnical engineers, and extensively for one-dimensional structures. Early studies in structural engineeringing showed that in general the shearing stress-shearing strain relationship can be represented analytically by the so-called Ramberg-Osgood (O-S) curves (Ramberg and Osgood, 1943), which involve three parameters, namely the shear modulus, the yielding stress value and the power of the ratio of the stress to the yielding value. These curves became widely used to represent hysteretical constitutive relationships, and although strictly speaking the nonlinear shear stress-strain relation of soft soils is represented by a hyperbola (Hardin and Drnevich 1972), soil engineers have frequently used R-O curves to represent soil columns, solving the wave equation by bilinear analysis or equivalent linear methods (Iddriss and Seed, 1968), and also by the method of characteristics (Streeter et. al 1974). The latter procedure was extended to two dimensions by arranging the basic one-dimensional element into a latticework. Similarly, Joyner and Chen (1975) and Joyner (1975) used the yielding element proposed by Iwan (1967) to study the nonlinear seismic response of one and two dimensional soil structures. As two-dimensional nonlinear analyses of ground response using models designed for yielding structures are beginning to find their way into soil engineering practice, our purpose in this paper is to investigate the similarities and differences of the responses computed with one of these methods and with a linear method for a prescribed 2-D problem. We choose a sediment filled valley and used a recorded earthquake to generate two amplitude input levels. The nonlinear and linear computations were performed independently by two teams among the authors, upon agreement of the problem specification and parameters. To some extent our objective is also to meet the seismological and engineering viewing of this classical problem.

NONLINEAR METHOD OF ANALYSIS

The method of analysis was developed by Joyner and Chen (1975) for one-dimensional structures, and by Joyner (1975) for two-dimensions, and will be presented here in outline. Modifications to the theory were made by incorporating a modified nonlinear soil model Larkin (1979) which is briefly described in this work.

The computational method uses an explicit finite difference scheme applied over a grid of discrete points chosen to model the valley, as shown in Figure 1. The soil mass is divided into a number of elements, either quadrilateral or triangular, and is underlain by a semi infinite elastic medium known with compression and shear wave velocities. This medium is the source of the input seismic energy. A transmitting boundary between both media is used to allow wave energy to return from the valley into the underlying halfspace. The computations are carried out in terms of particle velocity and two independent uncoupled solutions are achieved:

(i) *The in plane solution*, which solves for particle velocities V_1 and V_3, as shown in Figure 1, and is referred to as the PSV solution since it utilises the propagation of compression waves and in plane shear waves.

(ii) *The out of plane solution*, in which the dependent variable is V_2, as shown in Figure 1, and which is referred to as the SH solution since it utilises the propagation of shear waves causing out of plane distortions.

Analyses (i) and (ii) are carried out in terms of total stress and utilise the mean stress σ_m, and the deviatoric stress σ_{ij}, defined in equations (1) and (2), where the repeated index denotes demotion and δ_{ij} is the Kronecker delta.

$$\sigma_m = \frac{s_{kk}}{3} \tag{1}$$

$$\sigma_{ij} = s_{ij} - \sigma_m \delta_{ij} \tag{2}$$

Mean strain and deviatoric strain are defined in the same fashion as the stresses. The computations pass over the entire grid at each time step and velocity gradients are used to calculate the new values of strain. The values of stress are computed from the rheological model, described in the section that follows, from which forces and new velocities are obtained.

Constitutive Relationship

The stress - strain model used is based on classical incremental plasticity theory as described by Iwan (1967). The one dimensional version of this model has been used by Joyner and Chen (1975) and Taylor and Larkin (1978). Joyner (1975) developed the two dimensional version, which we take as the framework for the non-linear computations in the present study, with a modification that is described as follows (Larkin 1979).

The model uses a family of yield surfaces in stress space, each surface following the yield criteria of von Mises.

$$F_{a}\left(\sigma_{ij} - \alpha_{nij}\right) = k_{n}^{2} \tag{3}$$

where k_n is a characteristic of the n^{th} yield surface and α_{nij} is the origin of the surface in stress space. The total deviatoric strain e_{ij} consists of an elastic strain e_{Eij} plus a plastic strain component e_{pij} associated with the outer most yielding surface. This association of e_{pij} with the outer most yielding surface is a modification to the Iwan model (Larkin 1979). The Iwan model as used by Joyner (1975) has the concept of a plastic strain increment for each yield surface and sums the results for each surface that is associated with yielding. The modification results in savings of computing time of about 10-15%.

Kinematic hardening of the Prager type is used; that is, each yield surface translates in space and remains attached to the stress point on reaching yield until unloading occurs, so that

$$d\alpha_{nij} = c_n \, de_{pij} \tag{4}$$

where c_n is a constant associated with the n^{th} yield surface. The rule of flow normal to yield surfaces is invoked such that the plastic strain increments are normal to the corresponding yield surfaces. The relationship between mean stress and mean strain is assumed elastic.

$$de_m = \frac{d\sigma_m}{3K} \qquad (5)$$

where K is the bulk modulus.

The model may be based on laboratory data, such as dynamic torsion tests or cyclic simple shear tests. The values of k_n and c_n are then chosen to fit the laboratory data. Alternatively a hyperbolic stress-strain model (or any other suitable analytical or empirical relationship) may be used. The hyperbolic model has been widely used in soil dynamics and is described by Hardin and Drnevich (1972). In this study we use a hyperbolic initial loading curve to represent the dynamic properties of the alluvial valley.

The parameters required to specify the material properties are the low strain shear and compression wave velocities V_s and V_p, the undrained shear strength S_u and the mass density ρ. These are representative of parameters whose values are commonly measured in alluvial soils.

LINEAR METHOD OF ANALYSIS

The linear analysis was performed using the hybrid method presented by Benites and Haines (1991). A Riccati equation approach computes the wavefield within a heterogeneous region (Figure 2) resulting from any incident disturbance, and the Boundary - Integral Technique is used at the interface with the surrounding uniform medium to match the wavefields on the two sides of the interface, and thereby, incorporate a specified incident wavefield and generate the wavefield scattered into the uniform medium. The heterogeneous region can be of arbitrary shape and arbitrary material composition. The calculations are performed in the frequency domain and the time-domain solution is synthesised from independent solutions for a range of frequencies; i.e. $\underline{u}\,(\underline{x}, t) = \int \underline{u}\,(\underline{x}, \omega)\, e^{i\omega t} d\omega$. Any linear visco-elastic rheology can be considered. In particular, for the present study we used constant-Q dispersive attenuation:

$$\frac{1}{\mu(\omega)} = \frac{1}{\mu_\infty}\left[1 + \frac{1}{\pi Q_s}\ell n\left(-\frac{i\omega_\infty}{\omega}\right)\right]^2$$

$$\frac{1}{(\lambda + 2\mu)(\omega)} = \frac{1}{(\lambda + 2\mu)_\infty}\left[1 + \frac{1}{\pi Q_p}\ell n\left(-\frac{i\,\omega_\infty}{\omega}\right)\right]^2$$

where the S-wave quality factor inside the valley Q_s was chosen so that the visco-elastic damping of shear waves was comparable to the hysteretic damping in the non-linear analysis, and Q_p was assigned a value (twice Q_s) such that the decay of P waves with distance was very much less than the decay of S waves.

As it is explained in the Appendix, the Ricatti equation approach generates a set of displacement wavefields

$$\underline{u}_k\,(\underline{x},\omega)\ ,\quad k = 1,\ 2,\ \ldots$$

such that the complete seismic wavefield $\underline{u}\,(\underline{x},\,\omega)$ within the valley can be expressed as a superposition of these wavefields:

$$\underline{u}(\underline{x},\,\omega) = \sum_k \alpha_k\,(\omega)\;\underline{u}_k\,(\underline{x},\,\omega) \tag{6}$$

Each of the displacement fields $\underline{u}_k\,(\underline{x},\,\omega)$ and its associated tractions $\underline{\tau}_k\,(\underline{x},\,\omega)$ satisfy the elastodynamic equation. Because the rheology is linear the tractions associated with a combined displacement field (6) are

$$\underline{\tau}\,(\underline{x},\,\omega) = \sum_k \alpha_k\,(\omega)\;\underline{\tau}_k\,(\underline{x},\,\omega)$$

The coefficients α_k correspond to a particular incident wave $\underline{u}_o\,(\underline{x},\,\omega)$ and the wavefield $\underline{u}_s\,(\underline{x},\,\omega)$ scattered back into the surrounding medium, and are determined by satisfying boundary conditions at their interface. Using the Boundary Integral representation of the scattered wavefield (Ursell 1973) and the discretisation scheme based on source - point distribution, the total displacement and traction wavefield outside the valley can be written as

$$\underline{u}_h(\underline{x}, \omega) = \underline{u}_o(\underline{x}, \omega) + \sum_{\underline{x}_s} \underline{G}_u(\underline{x}, \underline{x}_s, \omega)\, F(\underline{x}_s, \omega)$$

$$\underline{\tau}_h(\underline{x}, \omega) = \underline{\tau}_o(\underline{x}, \omega) + \sum_{\underline{x}_s} \underline{G}_\tau(\underline{x}, \underline{x}_s, \omega)\, F(\underline{x}_s, \omega)$$

where $\underline{x}_s$ denotes the sources positions and $\underline{G}_u(\underline{x}, \underline{x}_s, \omega)$ and $\underline{G}_\tau(\underline{x}, \underline{x}_s, \omega)$ are the standard uniform-media displacement and traction Green's functions. The strengths of the sources $F(\underline{x}_s, \omega)$ and the coefficients for the valley $\alpha_k(\omega)$ are determined by minimising a weighted sum of squares

$$\sum_{\text{interface}} \left[W_u \left\{ \sum_k \alpha_k(\omega)\underline{u}_k(\underline{x}, \omega) - \left[\underline{u}_o(\underline{x}, \omega) + \sum_{\underline{x}_s} \underline{G}_u(\underline{x}, \underline{x}_s, \omega)\, F(\underline{x}_s, \omega) \right] \right\}^2 \right.$$

$$\left. + W_\tau \left\{ \sum_k \alpha_k(\omega)\underline{\tau}_k(\underline{x}, \omega) - \left[\underline{\tau}_o(\underline{x}, \omega) + \sum_{\underline{x}_s} \underline{G}_\tau(\underline{x}, \underline{x}_s, \omega)\, F(\underline{x}_s, \omega) \right] \right\}^2 \right]$$

corresponding to the mismatch of the boundary conditions at the interface between both regions, where W_u and W_τ are the weights assigned to displacements and tractions respectively.

The time-consuming part of the calculations is solving the Riccati equation to generate the set of independent wavefields

$$(\underline{u}_k, \underline{\tau}_k), \quad k = 1, 2, \ldots$$

inside the valley, but after these have been generated just once for a full set of frequencies, the above procedure can be used to obtain quickly the coefficients $\alpha_k(\omega)$ and $F(\underline{x}_s, \omega)$ for any number of incident wavefields with different time histories and different spatial distributions. For the present study, however, only one incident wavefield was considered for each rheology. Because of this and because the valleys were chosen purposely to be very simple, the full potential of the hybrid method was not exploited. The accuracy and power of the method have been demonstrated elsewhere (Benites and Haines 1991). The computation time depends on only the scale of the heterogeneity, in wavelengths, irrespective of the complexity of the problem.

Description of the Problem

The two dimensional basin modelled has a trapazoidal shape with a central depth H = 100 m and surface width L = 400 m. The so-called shape ratio H/L is therefore ¼. The shoulders have a constant slope of 45° as shown in Figure 3..

Two problems were analysed for this basin; the case of a homogeneous composition of the sediments and the case where the shear and compression velocities varied linearly from the ground surface to the bedrock.

The material properties for the homogeneous basin are:

V_s = 400 m/s

V_p = 2000 m/s

ρ = 1800 kg/m^3

s_u = 100 kPa

The value of Poisson's ratio is 0.48.

The material properties for the non-homogeneous basin are:

V_s = 200 - 400 m/s

V_p = 1500 - 2000 m/s

ρ = 1800 kg/m^3

s_u = 100 kPa

The value of Poisson's ratio is not constant.

The material properties of the bedrock assumed to underlay the basin are:

V_s = 2000 m/s

V_p = 3750 m/s

ρ = 2700 kg/m^3

with a value of 0.3 for Poisson's ratio.

Output from 16 points marked on Figure 2, at three depths in the basin was used to compare the nonlinear and linear results, and of these 16 points 5 in particular were used in detailed analyses. These points E, Q, C, M & B are also marked on Figure 2. Both in-plane (SH) and out-of-plane (PSV) analyses were carried out.

As input motion we used the ground acceleration recorded during the 1971 San Fernando Earthquake at the Castaic Old Ridge Route Station, California, USA. This record was chosen because it was recorded on firm bedrock and was of reasonable magnitude - peak horizontal acceleration 0.3 g. The earthquake record used has a duration of 50s in these analyses. The horizontal record was scaled to two levels of excitation to produce analyses at two strain levels. The high strain level has a peak input acceleration 0.4 g and the low strain level 0.04 g. The same scaling factors were applied to the vertical acceleration record. The same horizontal record was used for both in-plane and out-of-plane solutions, and the disturbance was taken to arrive vertically at the valley.

With the linear analysis the highest frequency was set to 5 Hz. This figure was then used to control the maximum nodal spacing in the nonlinear analysis. Higher frequencies will exist though in the nonlinear analysis and frequencies to 8 Hz will be represented with reasonable accuracy..

Initial runs were made with the nonlinear analysis to gauge the average levels of strain produced throughout the mesh over the whole analysis. This was done at both strain levels, and then this information was used to obtain the corresponding values of Q used in the linear analysis. These values were

High Strain	Q_s	=	3.125
Low Strain	Q_s	=	12.5

In addition, very low strain results are presented with $Q_s = 50$ for a case where the nonlinear analysis gave behaviour resembling undamped, linear elasticity. In all instances the value of the reference frequency ω_∞ for the constant-Q rheologies was chosen to be 5 Hz.

Output was obtained at the 16 points for all 3 components of motion, at two strain levels and for the two forms of material properties by both programs and the results were compared. The forms of output are:

Acceleration Time Histories and their Peak Valves

Acceleration Response Spectra with 5% damping

Fourier Spectra of the Acceleration time histories.

RESULTS

Fourier Spectra of the Acceleration Time Histories

Fourier Spectra for the quarter point Q in Figure 3 are shown in Figure 4 for both the PSV and SH solutions for the weak and strong events, and for both the uniform and non-uniform valleys. These spectra show a level of agreement between the linear and nonlinear analyses that is typical of the Fourier spectra we considered.

For frequencies up to 3 Hz, and sometimes higher, the spectral amplitudes are very similar, with both analyses predicting the same differences between the weak and strong events. Such agreement is not found in the acceleration time histories, the peak accelerations nor the response spectra. The likely explanation is that the Fourier spectral amplitudes are most strongly influenced in both methods by the same factors, in particular the geometry of the valley, distribution of wave velocities and the magnitude of the visco-elastic or hysteretic damping. The similarity of the spectra diminishes as the frequency increases. This is expected because the constant-Q damping in the linear analysis has its strongest effect at high frequencies, whereas with the nonlinear method there is a tendency for the highest frequencies to be amplified rather than attenuated, especially when the soil response is taking place at low strain. The high frequency response in the non-linear case is contaminated by numerical noise due to the finite difference scheme, as small artificial signals are generated whenever the strain level changes from one yield surface to another. While this effect is present, it is expected to be much less influential than the effects due to the fact that hysteretic damping is much less at low strain than at high strain.

The principal difference between the spectra for the weak and strong events is that for the weak event the spectra are characterised by a small number of large peaks, whereas, for the strong event the spectra shows many small peaks, reflecting the character of the input motion. The large peaks for the weak event are associated with site resonances which occur whenever seismic waves travelling by different paths arrive in phase at a particular point. The largest resonances occur when many different paths are involved, and cannot arise if each wave is heavily damped before it has been reflected many times within the valley. Consequently, the only easily identified resonances for the strong event are at the fundamental horizontal site period (1 second). In the linear case with the constant-Q rheology, it is known that attenuation with distance increases with increasing frequency, and for $Q_s = 3.25$, for instance, shear waves lose 60% of their amplitude every time they traverse one wavelength. The effects of hysteretic damping in the non-linear method are less understood, but given that the non-linear spectra for both events have the same features as those for the linear spectra, such effects must be similar to the effects of constant-Q damping in the build up of resonances. In particular, strong hysteretic damping on high strains prevents the focusing of wave energy in the same way that low-Q does.

The other consistent difference between the two events is the shift in the fundamental horizontal site period to a lower frequency for the strong event. The mechanism is different for the two analyses. For constant-Q rheology V_p and V_s decrease with decreasing frequency. The decrease in velocity is much more marked for the strong event with $Q_s = 3.25$ than for the weak event with $Q_s = 12.5$, and, of course, the fundamental period is inversely proportional to the shear -wave velocity. In the non-linear analysis there is also an effective decrease in velocity for the strong event, because at large strains the instantaneous tangent modulus is low.

For the weak event the SH nonlinear solution for the non-uniform valley shows an interesting effect when the strain level is very low. In this case the nonlinear method treats the medium as though it were linearly elastic with effectively no damping, and, as a result, there can be very large resonance peaks in the Fourier spectra. The corresponding linear solution for $Q_s = 50$ is shown in Figure 5. The amplitude variations are similar to the nonlinear case, though whereas in Figure 5 the peaks decrease in amplitude at high-frequency, this does not happen for the non-linear solutions. This may be an indication that the effective value of Q_s for the non-linear solution is higher than 50.

Response Spectra

Response spectra with 5% damping are shown in Figure 6 for the motion at Q, for the same complete set of solutions as the Fourier spectra in Figure 4.

It is clear from these excitation data that there are substantial differences between the linear and nonlinear solutions. This is an interesting observation considering the close similarity of the Fourier spectra. Seen from an engineering design point of view the two method of analysis would result in quite different estimates of base shear of a typical medium size building. Generally our observations show that the linear analysis yields response spectra that are of larger amplitude with more pronounced peaks. This may be due to the fact that an inherent characteristic of linear analyses is that wave energy never transfers from one frequency band to another while non-linear analyses produce such transfers of energy. Since the Fourier spectra for the two analyses are almost identical, these energy transfers in the nonlinear case must be counterbalanced some time later by energy transferring back to the original frequency band.

The time histories, discussed below, show the peak horizontal ground acceleration of the linear method to be larger than the nonlinear, yielding response spectra showing disparities particularly at the peaks, with the difference being a factor of 3 for the strong event and 2 for the weak event. This agrees with results from one-dimensional comparisons showing that as the strength of the event is increased the linear and non-linear methods produce diverging results.

In comparison with the nonlinear analysis the linear analysis amplifies the strength of the response at the fundamental horizontal site period (1 second) for both the horizontal components. Because the ratio H/L is not small enough for the valley to be effectively the same as a flat horizontal layer, both analyses predict that for the uniform basin there is a more dominant peak in the in-plane horizontal response at a period slightly smaller than the fundamental period, as shown particularly in the spectrum excited by the weak motion.

The response spectra of the vertical motions computed by the nonlinear and linear models show good agreement at short periods close to the peak in the spectra, although the spectra diverge for larger periods, with the linear spectra having consistently higher values. This difference is due to the effects of the boundaries of the valley since the vertical response spectra at the centre point C, shown in Figure 7 for the strong event, are in good agreement close to the peaks of the spectra and across the rest of the period range. The corresponding Fourier spectra, also shown in Figure 7, are in equally good agreement for frequencies less than 3 Hz, but the agreement is no better than for the Fourier spectra at the quarter point in Figure 4.

Acceleration Time Histories

An examination of the acceleration time histories in Figures 8 and 9 for the week and strong event yields the following major points. The corresponding peak accelerations for the labelled points E, Q, C, M and B are given in Table 1.

(i) The nonlinear analysis has a significantly higher content of energy in the high frequency range. We have already noted that this is to be expected since some of the soil response takes place at low strain levels where there is little hysteretic damping. Another contributing factor is the different high frequency bandwidths of the analyses. For the linear analysis the upper frequency limit was 5 Hz, whereas in the nonlinear case the response was modelled to approximately 8 Hz.

(ii) The linear analysis yields generally higher amplitudes, typically by a factor of 1.5. The reason the Fourier spectral amplitude of both linear and non-linear agree is that the duration of motion is also significantly different between the methods. The major effect is for the non-linear analyses to stretch the waveform and produce typically about twice the duration of the linear solution. This effect occurs because the wave front in nonlinear analyses propagates at the velocity associated with very low strain levels while the tail of the stress wave is moving at a much lower velocity associated with high-strain levels.

(iii) A difference between the results using the weak and strong input motions confirms the point already made about the magnitude of damping and its effect on the superposition of waves travelling by different paths to the same point. In the case of the strong motion (0.4g) both the linear and nonlinear results show little change in wave amplitude across the basin surface. In contrast, the results for the weak motion (0.04g) from both methods show a substantial increase in amplitude towards the centre of the basin. For both linear and non-linear analyses the waves excited by the strong input are much more damped than those when the input is weak. Consequently, amplifications resulting from superposition of waves travelling by paths of different lengths are likely to be much larger for the weak input motion than for the strong.

(iv) For strong and weak motion the nonlinear analysis gives marked deamplification at the edge point E, associated with stress concentrations at the sides of the valley (Larkin and Marsh 1991). It is possible that these stress concentrations act as barriers to the passage of waves from the valley into the surrounding medium.

(v) In the case of weak motion using the nonhomogeneous basin the nonlinear SH solution shows the pronounced resonance effect already remarked upon. Its manifestation in the time histories is the low amplitude (very low strain), long duration seismograms of uniform frequency content.

DISCUSSION AND CONCLUSIONS

Corresponding results for simple 2-dimensional alluvial basins have been obtained using linear modelling and the yielding-element model of non-linear behaviour proposed by Iwan (1967). It is establised that, though there are clear similarities in the character of the wave propagation for the two approaches, differences exist that are of primary importance for engineers, especially in regard to response spectra. The yielding-element non-linear model produces pronounced stretching of the time domain waveforms in the soils, resulting in lower peak accelerations and response spectra than that predicted by linear modelling. This is a consequence of different effective elastic moduli applying at different strain levels, so that as the strain changes at each point in the soil the phase and group velocities of waves passing through that point are altered. In particular, the effective moduli are less at high strain than at low strain. Whenever significant wave intensities build up the wave-forms move slower and, as this results in each wave packet becoming stretched over a longer interval of time, the amplitude of the packet diminishes, because of energy considerations. Such behaviour cannot be reproduced by linear modelling.

On the other hand, the Fourier spectra of the two sets of results are remarkably similar. From an engineering perspective, this means that linear modelling can predict accurately the total (time-integrated) intensity of shaking experienced by structures sited on soft soil deposits, even though the peak levels of shaking given by the response spectra may be overestimated. By choosing Q values giving the same average damping in the basins as the non-linear soils response for the weak and strong events, features of the non-linear wave propagation are reproduced. Resonace peaks obtained for the weak event are not present in the Fourier spectra for the strong event, because the greater damping of the high-strain case inhibits the formation of resonances. As a result, for the strong event the amplitudes of the time-histories are more uniform across the valley than the corresponding amplitudes for the weak event, which are larger in the centre than at the sides. The only clear resonance for the strong event is the fundamental resonance (about 1Hz) expected from the thickness of soil alone; that is, there is no clear focussing of energy resulting from the 2-dimensional nature of the basins. The frequencies for this peak in the Fourier spectra are smaller for the strong event than for the weak event, because the effective phase velocities are smaller. In the case of the linear method, the reduction in phase velocity results from the very small value of $Q_s (= 3.25)$ used for the strong event.

The points of agreement between the non-linear and linear results are in what can be termed "phase-velocity" phenomena, particularly resonances which occur when waves are in phase, whereas the main area of disagreement is assoiated with the group velocities at which packets of waves travel. The shapes of wave packets affect how fast they move and how much they are stretched in non-linear soils. An earthquake record is used as the input rock motion in this study. In future studies it is desirable that a variety of input pulse shapes, from very simple to very complicated be considered, to analyses their influence on the differences between linear and non-linear modelling.

APPENDIX:

Riccati Equation Approach

The details of the Riccati equation approach to the solution of the Elastodynamic equation are beyond the scope of the present paper. Relevant theory and properties of the solution are discussed in an internal monograph by Haines (1989). Papers on practical applications are in preparation. We will restrict ourselves to a brief description of the concepts involved.

The starting point is the choice of a range spatial variable ξ and either one cross-range spatial variable, η, for 2 dimensional problems or two cross-range variables for 3-dimensional problems. For valley problems ξ is a generalised depth co-ordinate, equal to 0 at the surface, 1 at the bottom of the first layer and so on, and η is a function of the horizontal position x (Figure A1). Let $\underline{n}$ be the downward unit normal to each of the surfaces S_ξ, such as the top and bottom of the valley, where ξ is constant, and dS_ξ denote increments of surface area, or line length in 2-D, on these surfaces. Now suppose

$$\phi_j(\eta), \quad j = 1, 2, \ldots$$

are an orthonormal set of basis functions for the valley; that is,

$$< \phi_j, \phi_k > = \int \phi_j(\eta)^* \, \phi_k(\eta) \, d\eta = \delta_{jk}.$$

At each point in the valley $\underline{x}(\xi, \eta)$ the components of displacement

$$u_p(\xi,\eta,\omega), \quad p = 1, 2, 3,$$

for each solution to the elastodynamic equation can be expanded as

$$u_p(\xi,\eta,\omega) = \sum_j U_{pj}(\xi,\omega) \, \phi_j(\eta) \tag{A1}$$

where

$$U_{pj}(\xi, \omega) = \int \phi_j^*(\eta) \, u_p(\xi, \eta, \omega) \, d\eta \, .$$

Likewise, the associated components of modified traction

$$\overline{\tau}_{p\xi}\ (\xi, \eta, \omega) \ = \ \frac{dS_\xi}{d\eta} \sum_q \tau_{\rho q}\ n_q$$

for the surfaces S_ξ can be written

$$\overline{\tau}_{p\xi}\ (\xi, \eta, \omega) \ = \ \sum_j T_{pj}\ (\xi, \omega)\ \phi_j(\eta) \tag{A2}$$

where

$$T_{pj}\ (\xi, \omega) \ = \ \int \phi_j^*\ (\eta)\ \overline{\tau}\ (\xi, \eta, \omega)\ d\eta\ .$$

Then the surface integrals like

$$\int_{S_\xi} \sum_p u_p^*\ (\xi, \eta, \omega) \sum_q \tau_{pq}\ (\xi, \eta, \omega)\ n_q\ dS_\xi$$

$$= \int \sum_p u_p^*\ (\xi, \eta, \omega)\ \overline{\tau}_{p\xi}\ (\xi, \eta, \omega)\ d\eta$$

can be converted into sums:

$$\begin{aligned} &\int \sum_p u_p^*\ (\xi, \eta, \omega)\ \tau_{p\xi}\ (\xi, \eta, \omega)\ d\eta \\ &= \sum_p \sum_j U_{pj}^*\ (\xi, \omega)\ T_{pj}\ (\xi, \omega)\ . \end{aligned} \tag{A3}$$

In particular, the total energy that flows through each surface on which ξ is constant is given by

$$- \int \left[\int_{S_\xi} \sum_p \frac{\partial u_p}{\partial t} (\underline{x}, t) \sum_q \tau_{pq} (\underline{x}, t)\, n_q \, dS_\xi \right] dt$$

$$= 2\pi \int \left[\int_{S_\xi} \sum_p i\,\omega\, u_p^* (\underline{x}, \omega) \sum_q \tau_{pq} (\underline{x}, \omega)\, n_q \, dS_\xi \right] d\omega \, .$$

The contribution each frequency makes to the total energy flow through the surfaces S_ξ is, therefore, proportional to the imaginary part of the sum (A3).

We will work in terms of the vectors $\underline{U}(\xi, \omega)$ and $\underline{T}(\xi, \omega)$, whose components $U_{pj}(\xi, \omega)$ and $T_{pj}(\xi, \omega)$, $p = 1,2,3$, $j = 1,2,\ldots$, are the coefficients in the expansions (A1) and (A2) of $u_p(\xi, \eta, \omega)$ and $\bar{\tau}_{p\xi}\ (\xi, \eta, \omega)$, and will denote the sum (A3) as $< \underline{U}(\xi, \omega), \underline{T}(\xi, \omega) >$. This is equivalent to working in terms of the functions $u_p\ (\xi, \eta, \omega)$ and $\bar{\tau}_{p\xi}\ (\xi, \eta, \omega)$, $p = 1,2,3$. The rheological law at each frequency giving the tractions as linear combinations of the spatial derivatives of the displacement field can be converted into an equation of the form.

$$\frac{d}{d\xi} \underline{U}(\xi, \omega) = \left[D_{uu}\right](\xi, \omega)\, \underline{U}(\xi, \omega) + \left[D_{u\tau}\right](\xi, \omega)\, \underline{T}(\xi, \omega) \qquad \text{(A4)}$$

where the matrices $\left[D_{uu}\right](\xi, \omega)$ and $\left[D_{u\tau}\right](\xi, \omega)$ involve the visco-elastic parameters for the medium and take account of the cross-range spatial derivatives of the displacements. Similarly, the elastodynamic equation, relating spatial derivatives of traction to acceleration, can be converted into

$$\frac{d}{d\xi} \underline{T}(\xi, \omega) = \left[D_{\tau u}\right](\xi, \omega)\, \underline{U}(\xi, \omega) + \left[D_{\tau\tau}\right](\xi, \omega)\, \underline{T}(\xi, \omega) \qquad \text{(A5)}$$

Henceforth the functional dependence on ξ and ω will be implicit.

Now let us check whether a general displacement field $\underline{U}$ can be split into independent displacement fields $\underline{U}_F$ and $\underline{U}_B$ for which the overall flows of energy through each of the surfaces S_ξ are respectively in the forward direction of increasing ξ and the opposite, backward direction. We write

$$\underline{U} = \underline{U}_F + \underline{U}_B, \quad \underline{T} = \underline{T}_F + \underline{T}_B .$$

Can we introduce matrices $[\Delta_F](\xi, \omega)$ and $[\Delta_B](\xi, \omega)$ such that at each value of the range variable ξ

$$\underline{T}_F(\xi, \omega) = [\Delta_F](\xi, \omega)\, \underline{U}_F(\xi, \omega),$$

$$\underline{T}_B(\xi, \omega) = [\Delta_B](\xi, \omega)\, \underline{U}_B(\xi, \omega)$$

and the two wavefields $\underline{U}_F$ and $\underline{U}_B$ are uncoupled, irrespective of the properties of the medium (provided, of course, that the rheology implies a linear relationship between displacement and traction)? One reason for doing this is that the directions of overall energy flow, either forward or backward, given by

$$\mathrm{Im} < \underline{U}_F, \underline{T}_F > \quad \text{and} \quad \mathrm{Im} < \underline{U}_B, \underline{T}_B >$$

for $\underline{U}_F$ and $\underline{U}_B$ respectively, are then controlled by the signs of the imaginary, or anti-Hermitian, parts of $[\Delta_F]$ and $[\Delta_B]$. Substituting into equation (A4) gives

$$\frac{d\underline{U}_F}{d\xi} + \frac{d\underline{U}_B}{d\xi} = \left\{[D_{uu}] + [D_{u\tau}]\,[\Delta_F]\right\} \underline{U}_F + \left\{[D_{uu}] + [D_{u\tau}]\,[\Delta_B]\right\} \underline{U}_B .$$

For $\underline{U}_F$ and $\underline{U}_B$ to be uncoupled this requires that

$$\frac{d\underline{U}_F}{d\xi} = \left\{[D_{uu}] + [D_{u\tau}]\,[\Delta_F]\right\} \underline{U}_F \qquad \text{(A6)}$$

and

$$\frac{d\underline{U_B}}{d\xi} = \left\{[D_{uu}] + [D_{u\tau}]\,[\Delta_B]\right\}\underline{U_B} \tag{A7}$$

Substituting into equation (A5):

$$\begin{aligned}
\underline{0} &= \frac{d\underline{T}}{d\xi} - \left\{[D_{\tau u}] + [D_{\tau\tau}]\,[\Delta_F]\right\}\underline{U_F} - \left\{[D_{\tau u}] + [D_{\tau\tau}]\,[\Delta_B]\right\}\underline{U_B} \\
&= \frac{d}{d\xi}\left\{[\Delta_F]\underline{U_F} + [\Delta_B]\underline{U_B}\right\} - \left\{[D_{\tau u}] + [D_{\tau\tau}]\,[\Delta_F]\right\}\underline{U_F} \\
&\qquad - \left\{[D_{\tau u}] + [D_{\tau\tau}][\Delta_B]\right\}\underline{U_B}\Big\} \\
&= [\Delta_F]\,\frac{d\underline{U_F}}{d\xi} + [\Delta_B]\,\frac{d\underline{U_B}}{d\xi} + \left\{\frac{d[\Delta_F]}{d\xi} - \left([D_{\tau u}] + [D_{\tau\tau}][\Delta_F]\right)\right\}\underline{U_F} \\
&\qquad + \left\{\frac{d[\Delta_B]}{d\xi} - \left([D_{\tau u}] + [D_{\tau\tau}][\Delta_B]\right)\right\}\underline{U_B}\,.
\end{aligned}$$

$$\begin{aligned}
&= \left\{\frac{d[\Delta_F]}{d\xi} + [\Delta_F]\left([D_{uu}] + [D_{u\tau}]\,[\Delta_F]\right) - \left([D_{\tau u}] + [D_{\tau\tau}][\Delta_F]\right)\right\}\underline{U_F} \\
&+ \left\{\frac{d[\Delta_B]}{d\xi} + [\Delta_B]\left([D_{uu}] + [D_{u\tau}][\Delta_B]\right) - \left([D_{\tau u}] + [D_{\tau\tau}][\Delta_B]\right)\right\}\underline{U_B}
\end{aligned}$$

which implies

$$\underline{0} = \left\{ \frac{d[\Delta_F]}{d\xi} + [\Delta_F]\left([D_{uu}] + [D_{u\tau}][\Delta_F]\right) - \left([D_{\tau u}] + [D_{\tau\tau}][\Delta_F]\right) \right\} \underline{U_F}$$

and

$$\underline{0} = \left\{ \frac{d[\Delta_B]}{d\xi} + [\Delta_B]\left([D_{uu}] + [D_{u\tau}][\Delta_B]\right) - \left([D_{\tau u}] + [D_{\tau\tau}][\Delta_B]\right) \right\} \underline{U_B},$$

if $\underline{U}_F$ and $\underline{U}_B$ are uncoupled.

Conversely, if $[\Delta_F]$ and $[\Delta_B]$ are independent solutions of the Riccati equation for matrices $[\Delta]$

$$\underline{0} = \frac{d[\Delta]}{d\xi} + [\Delta]\left([D_{uu}] + [D_{u\tau}][\Delta]\right) - \left([D_{\tau u}] + [D_{\tau\tau}][\Delta]\right) \tag{A8}$$

and are such that their anti-Hermitian parts are of the appropriate, opposite signs to ensure that the overall flows of energy forward and backward for $\underline{U}_F$ and $\underline{U}_B$ respectively, then, if $\underline{U}_F$ and $\underline{U}_B$ satisfy equations (A6) and (A7), the displacement, traction pairings

$$\underline{U_F}, \; \underline{T_F} = [\Delta_F]\,\underline{U_F}$$

and

$$\underline{U_B}, \; \underline{T_B} = [\Delta_B]\,\underline{U_B}$$

are independent, uncoupled solutions of the elastodynamic equation for the particular linear rheology being considered.

The above scheme has two advantages. First, it avoids the instability in other methods caused by not separating wavefields that decay in opposite directions (AboZena 1979). Energy considerations (to be precise, the second law of thermodynamics) ensure that numerical stability is assured when the Riccati equation (A8) is solved in the opposite direction to the overall energy flow associated with forward going $\underline{U}_F$ and backward going $\underline{U}_B$, and then equation (A6) and (A7) are solved in the direction of energy flow. In the case of $\underline{U}_F$, for example, for there to be overall flow of energy in the forward direction at ξ there has to be overall forward flow of energy at ξ - dξ, and, hence, the anti-Hermitian part of $[\Delta_F]$ can never go to zero. Furthermore, since the overall forward flow of energy associated with $\underline{U}_F$ cannot increase in the positive ξ direction, $\underline{U}_F$ must behave stably when equation (A6) is solved in this direction. For problems like the valleys considered in this paper it is necessary to have both a forward-going wavefield $\underline{U}_F$ and backward-going wavefield $\underline{U}_B$ so that the combined wavefield

$$\underline{U} = \underline{U_F} + \underline{U_B}, \quad \underline{T} = [\Delta_F]\,\underline{U_F} + [\Delta_B]\,\underline{U_B}$$

satisfies the free-surface boundary condition

$$\underline{T} = 0$$

and involves no nett vertical flow of energy there. Second, once a single pair of solutions $[\Delta_F]$ and $[\Delta_B]$ have been obtained to the Riccati equation (A8), equations (A6) and (A7) can be used to generate a full set of solutions

$$\underline{U_k} = \underline{U_{F,k}} + \underline{U_{B,k}}, \qquad k = 1, 2, \ldots\ldots$$

to the elastodynamic equation, each of which is for a different initial condition at the bottom of the valley, such that any other solution $\underline{U}$ can be expressed as a superposition of these solutions:

$$\underline{U} = \sum_k \alpha_k \, \underline{U_k}$$

and

$$\underline{T} = \sum_k \alpha_k \left\{ [\Delta_F] \, \underline{U_{F,k}} + [\Delta_B] \, \underline{U_{B,k}} \right\}.$$

REFERENCES

1. Darragh, R.B. and A.F. Shakal (1991), "The site response of two rock and soil station pairs to strong and weak ground motion", Bull. Seism. Soc. Am. 81, 1885 -1899.

2. Chin, B.H. and Aki, K. (1991), "Simultaneous study of the source, path and site effects on strong ground motion during the 1989 Loma Prieta earthqua: A preliminary results on pervasive nonlinear site effects", Bull. Seism. Soc. Am. 81, 1859-1884.

3. Aki, K. (1988), "Local site effects on strong ground motion", Earthquake Engineering and Soil Dynamics II - recent advances in ground motion evaluation, J.L Von Thun (Ed.), Geotechnical Special Publication No. 20, 103 - 155, Am. Soc. Civil Engr., New York.

4. Lee, V.W. (1978), "Displacement near a three-dimensional heimsperical canyon subjected to incident plane waves", Univ. of Sandiego Califotnia, Dept. of Civil Engineering, Report No. 78-16.

5. Lee, V.W. (1984), "Three-dimensional diffraction of plane P. SV and SH waves by a hemispherical alluvial valley", J. Soil Dyn. Earthq. Eng. 3(3), 133 - 144.

6. Lee, J.J. and Lanston, C.A. (1983), "Wave propagation in a three-dimensional circular basin", Bull. Seism. Soc. Am. 73, 1937 - 1953.

7. Sanchez-Sesma, F.J. (1983), "Diffraction of elastic waves by three-dimensional surface irregularities", Bull. Seism. Soc. Am. 73, 1621 - 1636.

8. Mossessian, T.K. and Dravinski, M. (1989), "Scattering of elastic waves by three dimensional surface topographics, wave motion, 579-592.

9. Mossessian, T.K. and Dravinski, M. (1989), "Amplification of elastic waves by a three dimensional valley", Part 1: Steady state response, Earthquake Engineering and Structural Dynamics 19, 667-680.

10. Ramberg, W. and Osgood, W.T. (1943), "Description of stress-strain curves by three parameters", Technical Note 902, National Advisory Committee for Aeronautics.

11. Hardin, B.O., and Drnevich, V.P. (1972), "Shear modulus and damping in soils: design equations and curves", Journal of the Soil Mechanics and Foundations Division, Am. Soc. Civil Engr. 98, No. SM7, Proc. Paper 9006, 667 - 692.

12. Idriss, I.M. and Seed, H.B. (1968), "Seismic response of horizontal soil layers", Proc. Am. Soc. Civil Engr., J. Soil Mech. Found. Div. 94, 1003-1031.

13. Streeter, V.L., Wylie, E.B. and Richart, F.E., (1974), "Soil motion computations by characterisitcs method", Proc. Am. Soc. Civil Engr., J. Geotech. Engr. Div. 100, 247 - 263.

14. Joyner, W.B. and T.F. Chen (1975), "Calculation of nonlinear ground response in earthquakes", Bull. Seism. Soc. Am. 65, 1315 - 1336.

15. Joyner, W.B. (1975), "A method for calculatub nonlinear seismic response in two-dimensions", Bull. Seism. Soc. Am. 65, 1337 - 1357.

16. Iwan, W.D. (1967), "On a class of models for the yielding behaviour of continuous and composite systems, Journal of Applied Mechanics 34, No. 4, 612-617.

Figure 1: Finite difference grid used in the non-linear analysis for the sedimentary basin described in the text. The mesh consists of rectangular and triangular elements, with modal spacing of m and time step s.

Figure 2: Domain representation of the hybrid method used in the linear analysis. The heterogenous region is shadowed, and the dots along the boundary represent artificial point wave sources. The arrows drawn at some of them depict scattered waves.

Figure 3: Geometry of the 2-D basin, showing the points where results from the non-linear and linear analyses were compared.

Figure 4: Fourier spectra from the linear (dashed) and non-linear (solid) analyses. The following coding is used to label the SH and PSV solutions: H = horizontal component, V = vertical component, Q = quarter point in Figure 3, U = homogeneous basin, N = non homogeneous basin with linear velocity gradient, S = strong event, W = weak event.

Figure 5: Fourier Spectrum of the linear SH solution at Q for the non-homogenous basin with $Q_s = 50$. For this value of Q_s the solution is denoted by Z, and the excitation level is set at 0.004 g, which is 10 times smaller than the excitation level for the weak event and 100 times smaller than the excitation level for the strong event.

Figure 6: Response spectra with 5% damping for the SH and PSV solutions at Q. The coding is the same as in Figure 4.

Figure 7. Response spectra with 5% damping and Fourier spectra for the vertical component of the PSV solution at the centre point C in Figure 3 for the strong event. Spectra are shown for both the homogeneous basin (U) and the non-homogenous basin (N).

Figure 8: SH accelerations for the strong event, at all the points indicated in Figure 3, obtained with the non-linear and linear methods. time histories are shown for both the homogenous basing (U) and the non-homogenous basin (N).

Figure 9: SH accelerations for the weak event, presented like in Figure 8.

Figure A1: Co-ordinate system used in the Riccati approach, showing surfaces on which the range co-ordinate ξ is constant.

Table 1: Peak positive and negative accelerations at the labelled points in Figure 3, predicted for the strong and weak events by the non-linear (NL) and linear (L) methods. Values for the homogeneous basin (uniform mesh) are presented first, followed by the values for the non-homogenous basin (linear gradient mesh).

TYPICAL BASIN MESH

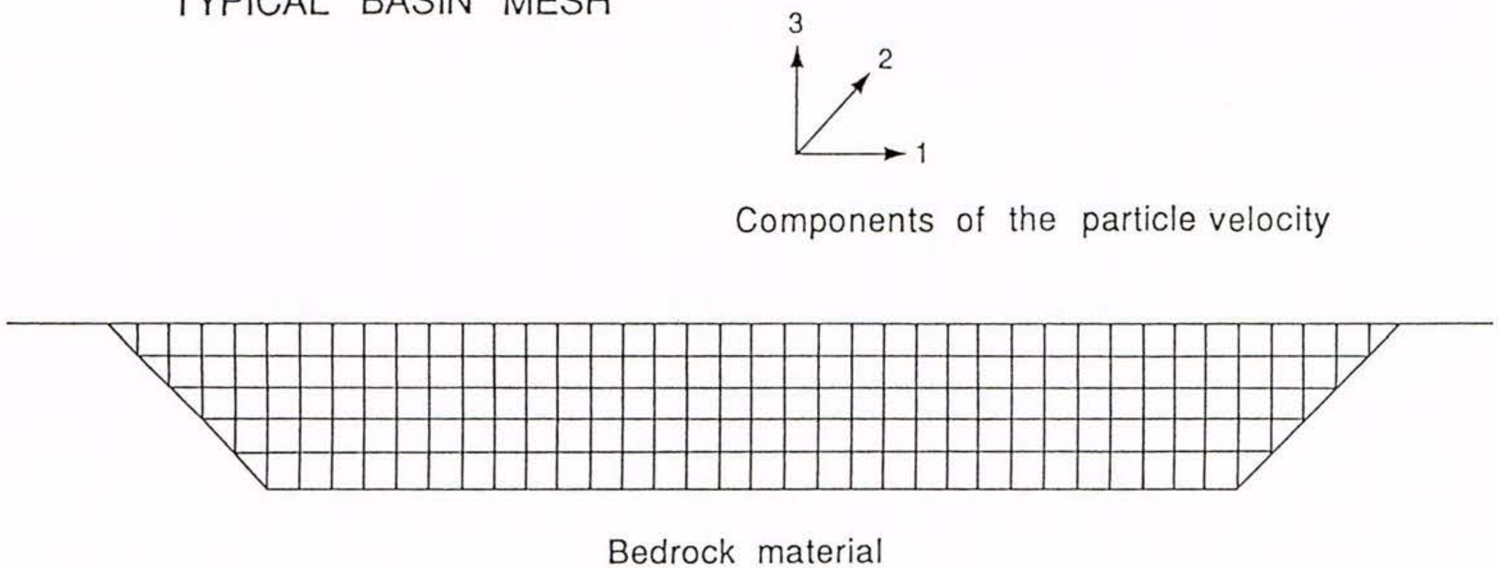

Figure 1

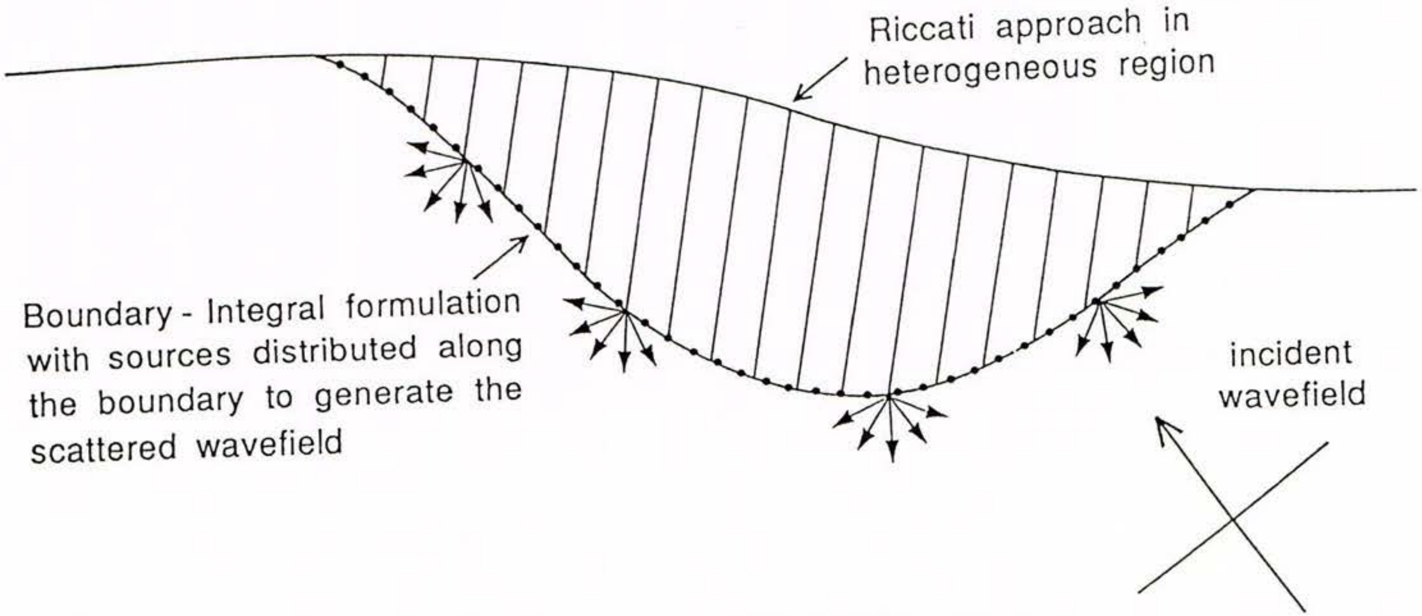
Riccati approach in heterogeneous region
Boundary - Integral formulation with sources distributed along the boundary to generate the scattered wavefield
incident wavefield

Figure 2

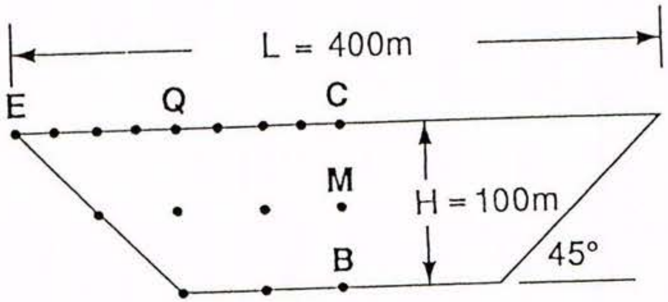

Figure 3

FOURIER AMPLITUDE SPECTRUM

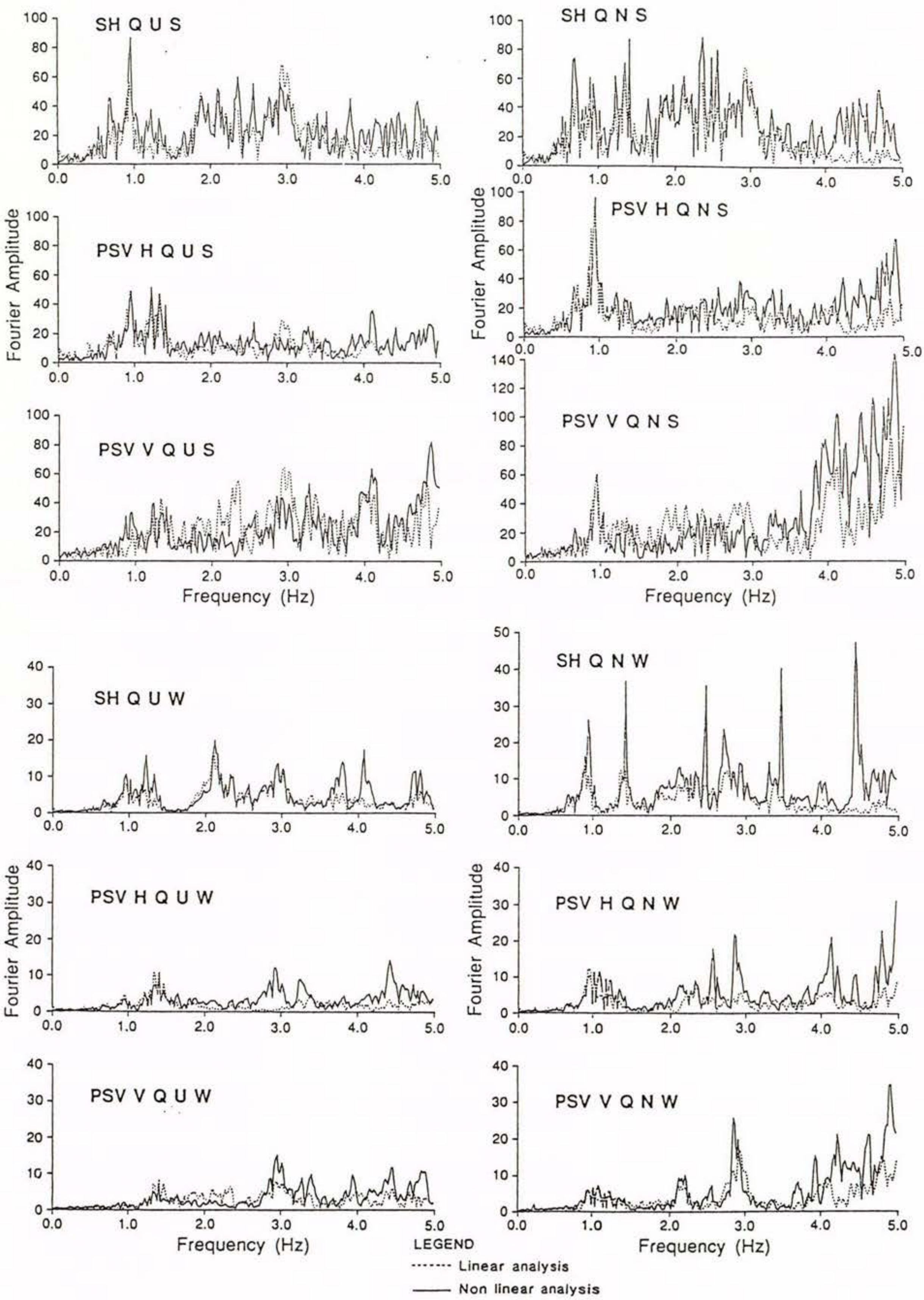

Figure 4

FOURIER AMPLITUDE SPECTRUM

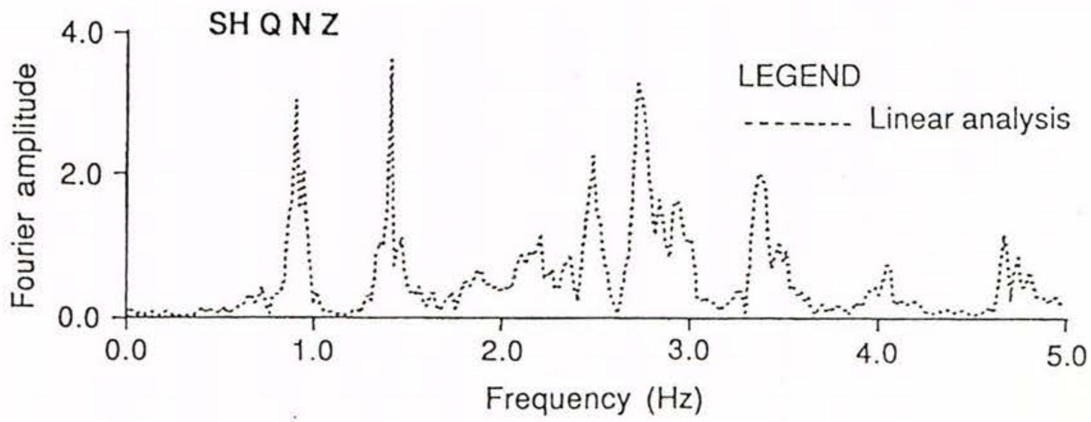

Figure 5

SURFACE ACCELERATION RESPONSE SPECTRUM

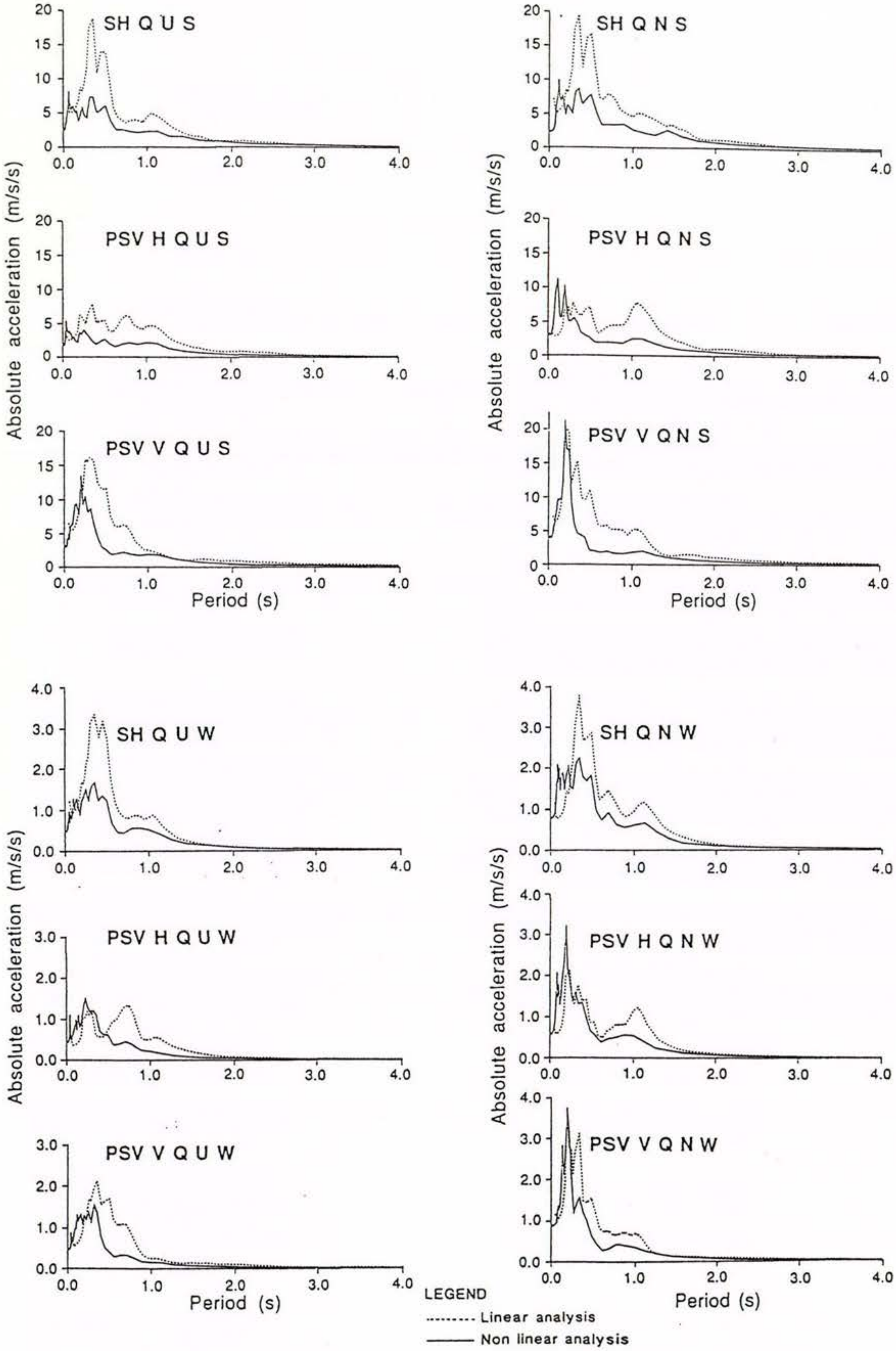

Figure 6

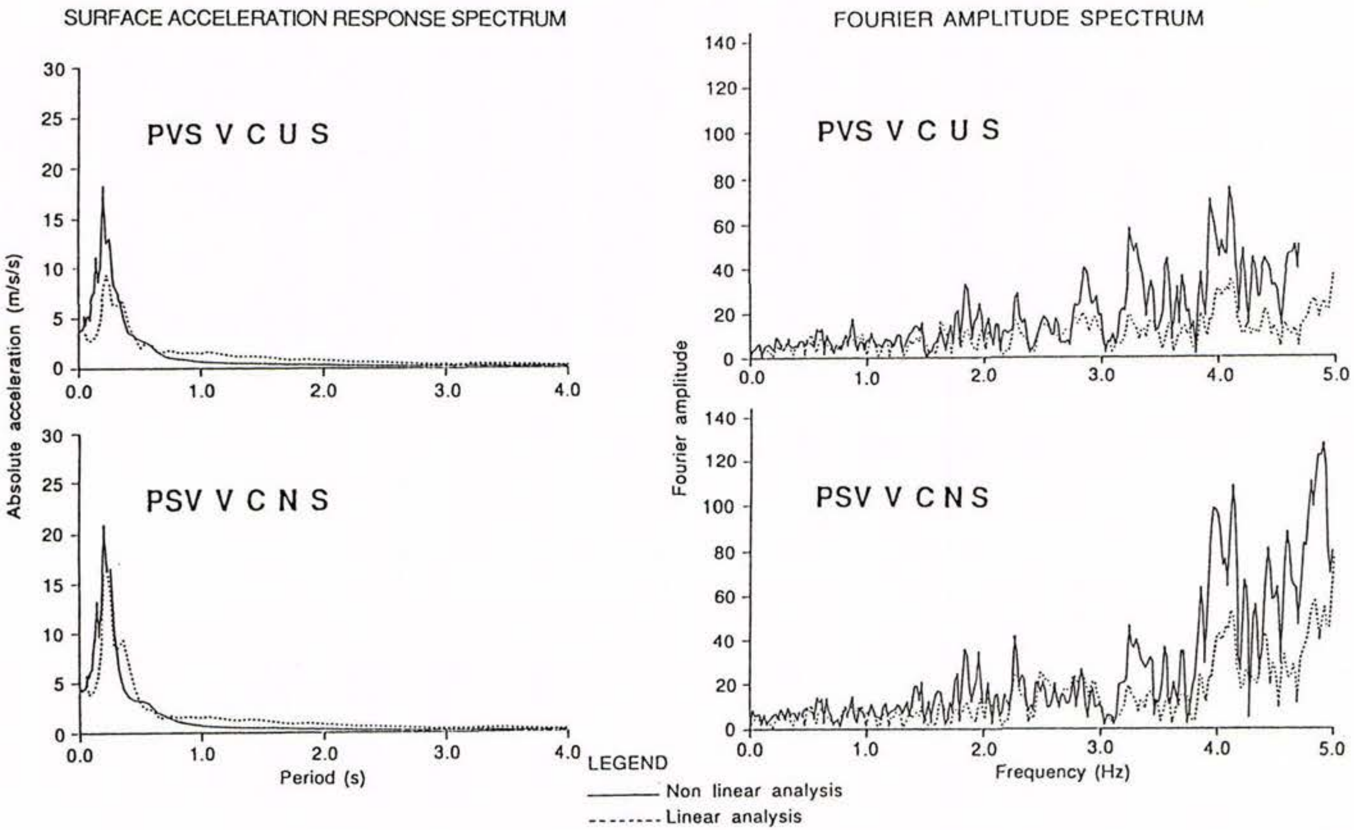
SURFACE ACCELERATION RESPONSE SPECTRUM
FOURIER AMPLITUDE SPECTRUM
PVS V C U S
PSV V C N S
Absolute acceleration (m/s/s)
Period (s)
Fourier amplitude
Frequency (Hz)
LEGEND
Non linear analysis
Linear analysis

Figure 7

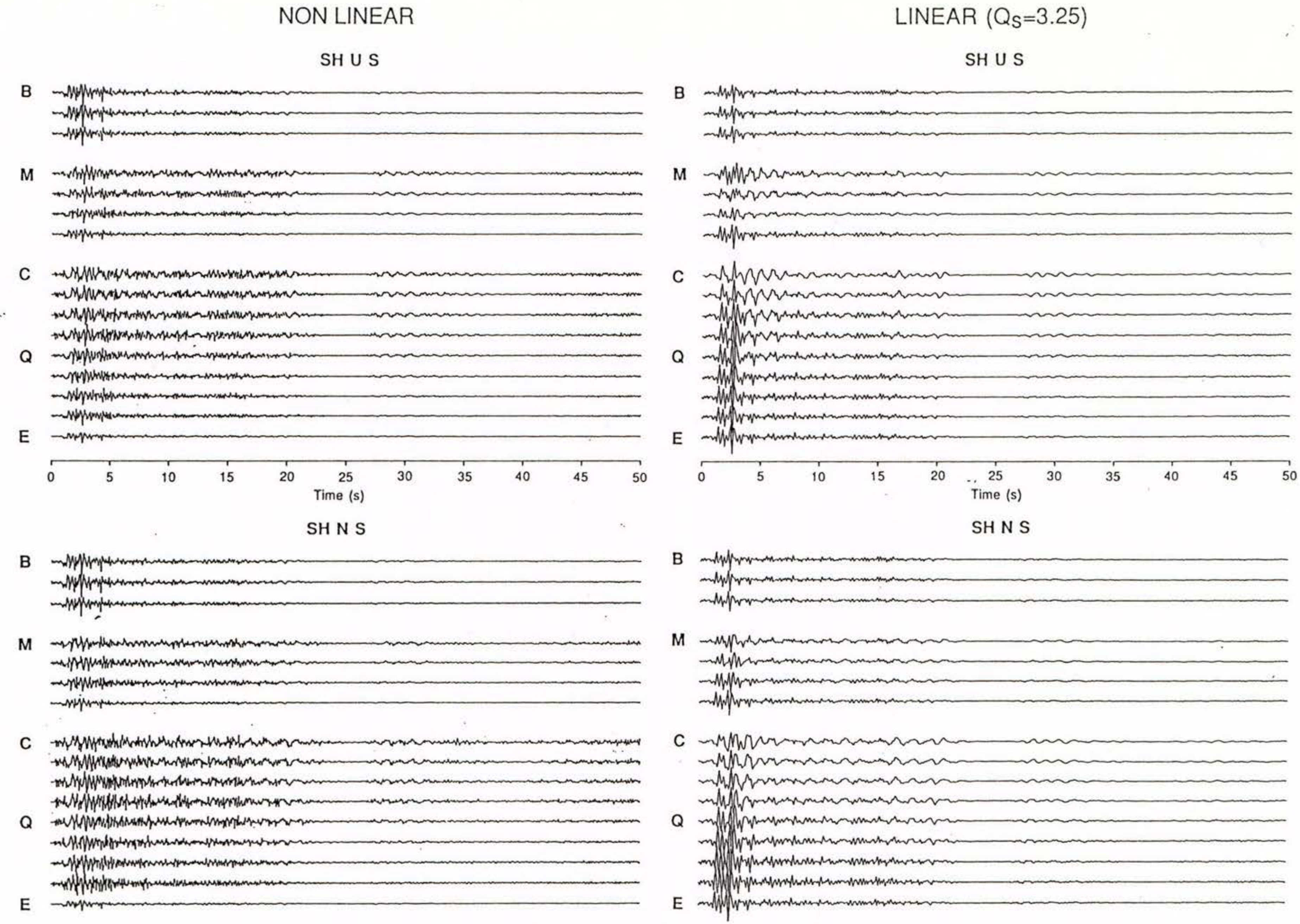
NON LINEAR
LINEAR (Q_S=3.25)
SH U S
B
M
C
Q
E
0 5 10 15 20 25 30 35 40 45 50
Time (s)
SH N S

Figure 8

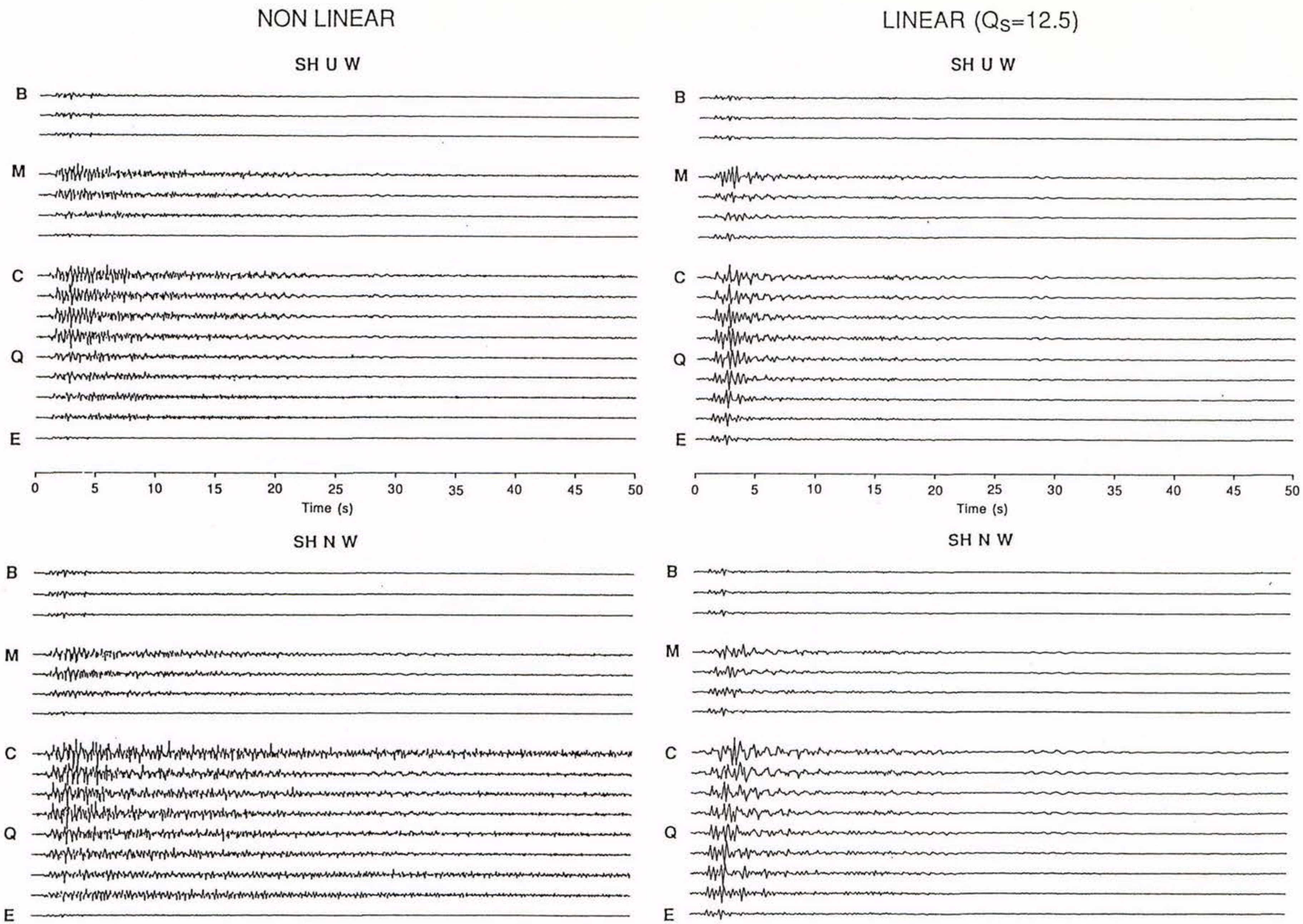

NON LINEAR
LINEAR (Q_S=12.5)
SH U W
SH N W
B
M
C
Q
E
0
5
10
15
20
25
30
35
40
45
50
Time (s)

Figure 9

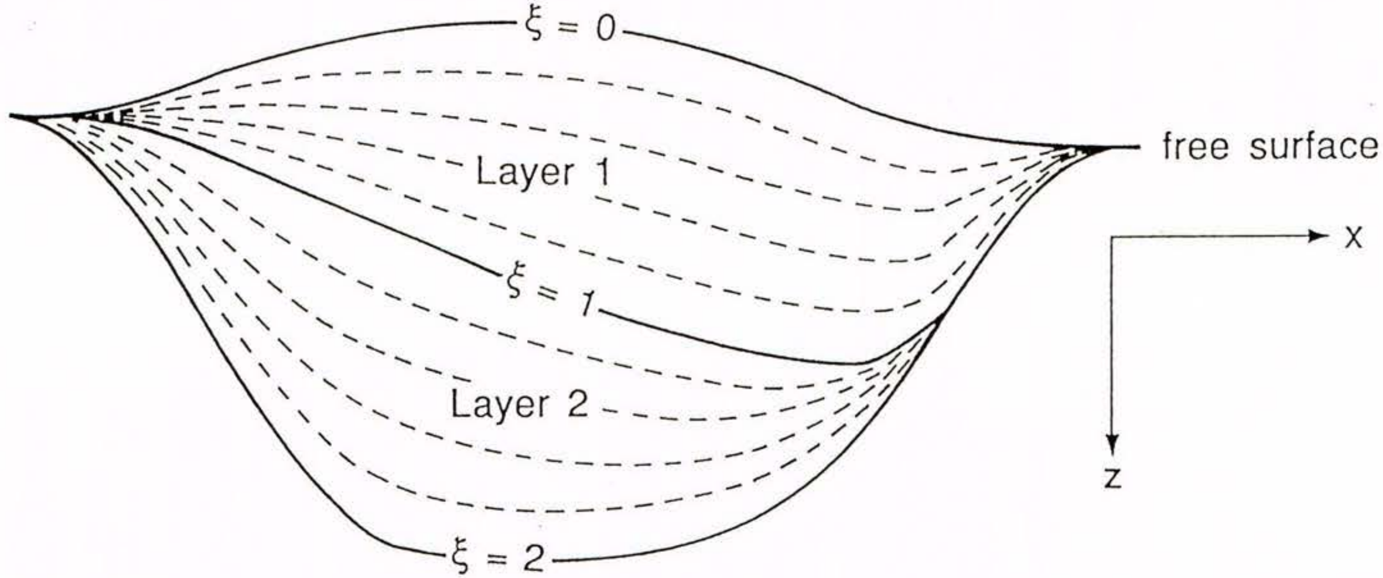

Figure A1

UNIFORM MESH STRONG							PEAK ACCELERATIONS (m/s^2) WEAK						
			NL			L				NL			L
SH	C	+	2.51		+	3.55			+	0.80		+	0.94
		-	2.14		-	2.58			-	1.13		-	0.65
	Q	+	2.08		+	4.18			+	0.46		+	0.68
		-	2.50		-	4.45			-	0.48		-	0.83
	E	+	0.98		+	3.00			+	0.11		+	0.32
		-	1.61		-	4.14			-	0.16		-	0.42
	M	+	2.37		+	3.02			+	0.80		+	0.82
		-	2.75		-	2.69			-	0.68		-	0.91
	B	+	2.16		+	1.92			+	0.24		+	0.19
		-	3.64		-	2.64			-	0.35		-	0.26
PSV_H	C	+	2.09		+	3.15			+	0.63		+	0.55
		-	2.85		-	4.12			-	0.99		-	0.79
	Q	+	1.50		+	2.57			+	0.42		+	0.36
		-	1.65		-	2.00			-	0.42		-	0.31
	E	+	0.56		+	2.50			+	0.063		+	0.27
		-	0.57		-	2.74			-	0.067		-	0.35
	M	+	2.01		+	2.06			+	0.37		+	0.32
		-	1.52		-	2.14			-	0.60		-	0.41
	B	+	2.14		+	2.23			+	0.22		+	0.23
		-	3.69		-	2.24			-	0.34		-	0.24
PSV_V	C	+	3.12		+	2.55			+	0.54		+	0.38
		-	3.71		-	1.95			-	0.47		-	0.36
	Q		2.67		+	4.72			+	0.40		+	0.50
			2.90		-	5.30			-	0.46		-	0.57
	E		1.15		+	1.98			+	0.11		+	0.24
			1.20		-	1.55			-	0.12		-	0.18
	M		2.48		+	2.15			+	0.38		+	0.31
			2.44		-	1.66			-	0.44		-	0.22
	B		1.43		+	1.38			+	0.15		+	0.13
			1.28		-	1.07			-	0.14		-	0.12

LINEAR GRADIENT MESH STRONG							PEAK ACCELERATIONS (m/s^2) WEAK						
			NL			L				NL			L
SH	C	+	2.61		+	2.72			+	1.11		+	1.03
		-	2.52		-	2.55			-	1.49		-	1.00
	Q	+	2,11		+	4.10			+	0,59		+	0.68
		-	2,30		-	5.11			-	0.78		-	0.69
	E	+	1.30		+	3.38			+	0.10		+	0.34
		-	1.65		-	4.53			-	0.16		-	0.45
	M	+	2.60		+	1.71			+	0.59		+	0.62
		-	2.73		-	2,86			-	0.75		-	0.56
	B	+	2.12		+	2.36			+	0.22		+	0.25
		-	3.65		-	3.03			-	0,33		-	0.32
PSV_H	C	+	2.57		+	3.30			+	0.94		+	0.84
		-	2.33		-	3.32			-	0.78		-	0.87
	Q	+	2.92		+	2.42			+	0.58		+	0.48
		-	2.48		-	2.54			-	0,53		-	0.52
	E	+	0.55		+	2.71			+	0.050		+	0,27
		-	0.57		-	3.63			-	0.059		-	0.36
	M	+	2,05		+	1.35			+	0,31		+	0.27
		-	2.08		-	1.98			-	0.54		-	0,36
	B	+	2.05		+	2,15			+	0.22		+	0.22
		-	3.63		-	2.38			-	0,34		-	0.25
PSV_v	C	+	4.10		+	3.59			+	0.60		+	0.48
		-	3.66		-	2,92			-	0.65		-	0.46
	Q	+	3.38		+	5.81			+	0.87		+	0.99
		-	3.96		-	4.10			-	0.86		-	0.78
	E	+	1.11		+	2.44			+	0.11		+	0.24
		-	1.18		-	1.91			-	0.12		-	0.19
	M	+	2.47		+	2.74			+	0.39		+	0.28
		-	2.54		-	1.94			-	0.36		-	0.25
	B	+	1.32		+	1.40			+	0.13		+	0.13
		-	1.35		-	1.22			-	0.15		-	0.11